

# IMPORTANT CONSIDERATIONS FOR LOCATING BURIED AGRICULTURAL DRAINAGE PIPE USING GROUND PENETRATING RADAR

B. J. Allred, J. J. Daniels, N. R. Fausey, C. Chen, L. Peters, Jr., H. Youn

**ABSTRACT.** *Enhancing the efficiency of soil water removal on land already containing a subsurface drainage system typically involves installing new drain lines between the old ones. However, the older drainage pipes need to be located before this approach can be attempted. In ongoing research, a near-surface geophysical method, ground penetrating radar (GPR), has been successful in locating on average 72% of the total amount of drainage pipe present at 13 test plots in southwest, central, and northwest Ohio. The effective use of GPR for drainage pipe detection requires careful consideration of computer processing procedures, equipment parameters, site conditions, and field operations, all of which were thoroughly investigated in this study.*

*Application of a signal saturation correction filter along with a spreading and exponential compensation gain function were the computer processing steps most helpful for enhancing the drainage pipe response exhibited within GPR images of the soil profile. GPR amplitude maps that show the overall subsurface drainage pipe system required additional computer processing, which included 2-D migration, signal trace enveloping, and in some cases, a high frequency noise filter and a spatial background subtraction filter. Equipment parameter test results indicate that a 250-MHz antenna frequency worked best, and that data quality is good over a range of spatial sampling intervals and signal trace stacking. In regard to the site conditions present, shallow hydrology, soil texture, and drainage pipe orientation all substantially influence the GPR response. Additionally, drainage pipe that are as small as 5 cm (2 in.) in diameter can be detected. However, the fired clay or plastic material of which the drainage pipe is comprised does not appear to have much of an impact. Finally, with respect to GPR field operations, bidirectional surveys offer the best chance for finding all the buried drainage pipe possible, and for displaying a subsurface drainage system on an amplitude map, the narrower the spacing between GPR measurement lines, the better the result. Although it is important to note that the amplitude maps generated with a wider spacing between GPR measurement lines, still provided plenty of useful data on drainage pipe location. The information supplied by this study can be employed to formulate guidelines that will enhance the potential of success for using ground penetrating radar in locating buried agricultural drainage pipe.*

**Keywords.** *Agricultural drainage pipe, Near-surface geophysics, Ground penetrating radar, Computer processing procedures, Equipment parameters, Site conditions, Field operations.*

**A** 1985 economic survey (USDA Economic Research Service, 1987) showed that the states comprising the Midwest United States (Illinois, Indiana, Iowa, Ohio, Minnesota, Michigan, Missouri, and Wisconsin) had by that year approximately 12.5 million ha (31 million acres) that contained subsurface

drainage systems. Cropland constituted by far the large majority of this acreage. The same economic survey estimated the 1985 on-farm replacement cost for these cropland subsurface drainage systems to be \$18 billion (US). Today, this subsurface drainage infrastructure would be worth \$30 billion (US), based on a 1986–2002 average yearly consumer price index inflation rate of 3.1%, and this total does not include the extensive amount of drainage pipe that has been installed since 1985. The magnitude of the acreage involved along with infrastructure costs indicate how crucial subsurface drainage is to the Midwest U.S. farm economy, without which, excess soil water could not be removed, in turn making current levels of crop production impossible to achieve.

Prior to the 1960s, agricultural drainage pipe was constructed primarily of clay tile, and to a lesser extent, concrete tile. Clay tile drainage pipes were fabricated in a three-stage molding, firing, then cooling process and typically produced in 30-cm (12-in.) long segments having inside diameters of either 10 or 15 cm (4 or 6 in.). Substantial variability is often seen in cross-sectional shape. These segments were laid down end-to-end in an excavated trench, and in Ohio, where this study was conducted, buried at depths usually between 0.5 and 1 m (1.5 and 3 ft). During drainage,

---

Article was submitted for review in November 2003; approved for publication by the Soil & Water Division of ASAE in July 2004. Presented at the 2003 ASAE Annual Meeting as Paper No. 032344.

The use of product names is for information purposes only and does not imply endorsement by the authors or the organizations they represent.

The authors are **Barry J. Allred**, ASAE Member, Agricultural Engineer, USDA/ARS Soil Drainage Research Unit, Columbus, Ohio; **Jeffrey J. Daniels**, Professor, Department of Geological Sciences, Ohio State University, Columbus, Ohio; **Norman R. Fausey**, ASAE Member, Research Leader, USDA/ARS Soil Drainage Research Unit, Columbus, Ohio; **Chi-Chih Chen**, Senior Research Associate, ElectroScience Laboratory, **Leon Peters, Jr.**, Emeritus Professor, ElectroScience Laboratory, and **Hyoungh-Sun Youn**, Graduate Student, Electrical Engineering Department, Ohio State University, Columbus, Ohio. **Corresponding author:** Barry J. Allred, USDA/ARS Soil Drainage Research Unit, 590 Woody Hayes Dr., Room 234, Columbus, OH 43210; phone: 614-292-9806; fax: 614-292-9448; e-mail: allred.13@osu.edu.

most of the water removed from the soil enters the clay tile pipe through joints between segments. Concrete tile was only used in areas where a good source of clay was unavailable for pipe construction.

In the 1960s, clay and concrete tile were superseded by corrugated plastic tubing (CPT), which is still today the material most commonly used in drainage pipe (Schwab et al., 1981). The corrugations provide bearing strength and pipe flexibility. In the United States, high-density polyethylene is used for CPT construction and tubing is extruded and then packaged in long coils. The most common inside diameter for plastic drainage pipe is 10 cm (4 in.). The drainage installation equipment now in use has enabled trenching, CPT emplacement, and backfilling operations all to be conducted concurrently. The burial depth for newer corrugated plastic tubing, at least in Ohio, averages around 1 m (3 ft). Drainage waters enter the plastic tubing through perforations.

Figure 1 is a schematic illustrating drainage pipe placement within the soil profile typical of agricultural fields in Ohio. The tilled zone is commonly less than 0.3 m (1 ft) in thickness. The pipe is emplaced at the bottom of the trench, which is then backfilled. The trench itself is typically 0.3 to 0.5 m (1 to 1.5 ft) wide with its bottom depth ranging between 0.5 and 1 m (1.5 and 3 ft). The water table can be either above or below the drainage pipe depending on the amount of recent rainfall and the mode of operation for the subsurface drainage system (uncontrolled drainage, controlled drainage, or subirrigation).

Increasing the efficiency of soil water removal on farmland that already contains a functioning subsurface drainage system often requires reducing the average spacing distance between drain lines. This is typically accomplished by installing new drain lines between the older ones. By keeping the older drain lines intact, less new drainage pipe is needed, thereby substantially reducing costs to farmers.

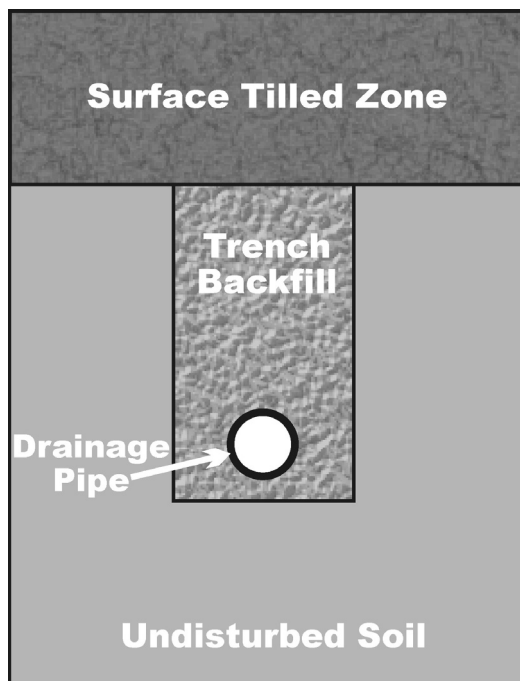


Figure 1. Schematic of the drainage pipe position within the soil profile.

However, before this approach can be attempted, the older drain lines need to be located. Subsurface drainage pipe also needs to be found prior to construction project initiation on present or former farmland. Before construction begins, subsurface drainage system alteration is frequently necessary to avoid water ponding problems at the surface resulting from inadvertent damage to a buried drainage pipe.

Regardless of the need, finding drainage pipe is not an easy task, especially for systems installed more than a generation ago. Often, records have been lost, and the only outward appearance of the subsurface drainage system is a single pipe outlet extending into a water conveyance channel. From this observation of the outlet, little can be deduced about the network pattern used in drainage pipe placement. Without records that show precise locations, finding a drain line with heavy trenching equipment causes pipe damage requiring costly repairs, and the alternative of using a hand-held tile probe rod is extremely tedious at best. Satellite or airborne remote sensing technologies show some promise (Zucker and Brown, 1998) but are only applicable during certain times of the year and under limited site conditions.

Consequently, there is definitely a need to find better ways of effectively and efficiently locating buried agricultural drainage pipe. Conventional near-surface geophysical methods, such as those commonly used for environmental and construction-engineering applications, have the potential to successfully address this need. Though surprisingly, little work has been done on this topic, especially in the Midwest United States. Chow and Rees (1989) demonstrated the use of ground penetrating radar (GPR) to locate subsurface agricultural drainage pipes in the Maritime Provinces of Canada, and Boniak et al. (2002) showed that GPR could be employed to find drainage pipe beneath golf course greens. However, the use of geophysical methods to locate buried plastic or metal utility pipelines has been studied in much greater detail. Promising results have been achieved with GPR (LaFaleche et al., 1991; Wensink et al., 1991; Zeng and McMechan, 1997; Hayakawa and Kawanaka, 1998), electromagnetic induction (Chen et al., 1991), and resistivity (Zhang and Luo, 1991) surveying techniques. During the 1970s and 1980s, the ElectroScience Laboratory at Ohio State University developed a ground penetrating radar system capable of finding 60% of plastic utility pipes in 60% of the United States (Young and Caldecott, 1976; Peters and Young, 1986). Furthermore, fired clay objects at shallow depth have been detected with geomagnetic surveys (Sharma, 1997).

Recent drainage pipe detection research by Allred et al. (2004) indicated that of the four different geophysical methods tested (geomagnetic surveying, electromagnetic induction, resistivity, and ground penetrating radar) the only one of promise was ground penetrating radar (GPR). In addition, GPR grid surveys have been conducted in southwest, central, and northwest Ohio at 13 test plots containing subsurface drainage systems, and with respect to locating the total amount of pipe present at each site, this technology was shown to have an average effectiveness of 72% (100% of the pipe was found at six sites, 90% at one site, 75% at two sites, 50% at two sites, and 0% at two sites.) On the whole, this method was reasonably successful in finding clay tile and corrugated plastic tubing drainage pipe down to depths of around 1 m (3 ft).

The new governing hypothesis for the ongoing research program was that computer processing procedures, equipment parameters, site conditions, and field operations are all important, and therefore need to be carefully considered for successful employment of ground penetrating radar to detect agricultural drainage pipe. A signal saturation correction filter, gain functions, 2-D migration, signal trace enveloping, a high frequency noise filter, and a spatial background subtraction filter were the computer processing procedures assessed. The tested GPR equipment parameters included antenna frequency, spatial sampling interval, and signal trace stacking. The influence of site conditions on GPR response were studied with respect to shallow hydrology, soil texture, drainage pipe orientation, drainage pipe material, and drainage pipe diameter. The field operations addressed included unidirectional versus bidirectional GPR surveying and the spacing distance between lines of GPR measurement. The overall objective for this research is to use the information collected to develop guidelines that will enhance the success of using ground penetrating radar to locate buried agricultural drainage pipe.

## MATERIALS AND METHODS

The principle of the ground penetrating radar (GPR) method involves directing an electromagnetic radio energy (radar) pulse into the subsurface, followed by measurement of the elapsed time taken by the signal as it travels downwards from the transmitting antenna, partially reflects off a buried feature, and is eventually returned to the surface, where it is picked up by a receiving antenna. Reflections from different depths produce a signal trace, which is a function of radar wave amplitude (and energy) versus time. Antenna frequency, soil moisture conditions, clay content, salinity, and the amount of iron oxide present all have a substantial influence on the distance beneath the surface to which the radar signal penetrates.

Differences in the dielectric constant across a discontinuity, govern the amount of radar energy that reflects off the discontinuity interface, and accordingly, the amount of radar energy transmitted through the interface (fig. 2). The ratio of the reflected radar pulse amplitude to the incident radar pulse

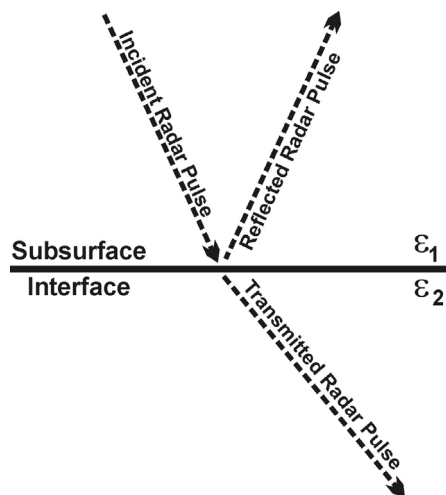


Figure 2. Schematic of the radar pulse interaction at a subsurface dielectric constant discontinuity.

amplitude is given by the reflection coefficient, R, which can be expressed quantitatively as follows:

$$R = \frac{\sqrt{\epsilon_2} - \sqrt{\epsilon_1}}{\sqrt{\epsilon_2} + \sqrt{\epsilon_1}} \quad (1)$$

where  $\epsilon_1$  is the dielectric constant of the medium in which the radar pulse is currently traveling, and  $\epsilon_2$  is the dielectric constant of the medium across the discontinuity interface. A negative reflection coefficient value implies that the reflected radar pulse polarity has been reversed. The greater the absolute value of the reflection coefficient, the more energy is reflected. (The actual radar energy reflected is proportional to  $R^2$ .)

For this study, there are two obvious dielectric constant discontinuities. One is the interface between the drainage pipe and surrounding soil material and the second is the interface between the drainage pipe and the air/water within it (fig. 1). However, if the drainage pipe wall thickness is small relative to the radar pulse wavelength (definitely the case for corrugated plastic tubing and likewise for clay tile), then as a result of constructive or destructive interference between the radar pulses reflected off the outer and inner walls of the pipe, the effective GPR reflection response essentially becomes governed by the dielectric constant values of the surrounding soil material and the air/water inside the pipe (Sensors & Software Inc., personal communication, 27 October 2003).

The dielectric constant ranges in value from 1 for air to 80 for water with dry soil closer to the lower end of this range, ~5 to 15, and very moist or saturated soils near the middle of the range, ~30 to 40 (Sutinen, 1992; Conyers and Goodman, 1997; Reynolds, 1997; Sharma, 1997). The dielectric constant,  $\epsilon$ , of soil material is directly dependent on the volumetric moisture content,  $\theta$ . The relationship between  $\epsilon$  and  $\theta$  was empirically developed for soils in general by Topp et al. (1980) and is given by:

$$\epsilon = 3.03 + 9.03(\theta + 146.0(\theta^2)) - 76.7(\theta^3) \quad (2)$$

A second equation empirically developed by Sutinen (1992) for glacial materials, such as those found in the Midwest United States, is expressed:

$$\epsilon = 3.2 + 35.4(\theta + 101.7(\theta^2)) - 63(\theta^3) \quad (3)$$

If the clay tile pipe does not readily absorb water then it will most likely have a dielectric constant value within the range of 3 to 7 (Chemical Rubber Company, 1994; Sharma, 1997), but if it is capable of significant water absorption then the pipe will probably have a value similar to the soil around it. A clay tile pipe having a dielectric constant similar to the soil enclosing it will essentially be “transparent” to GPR. The dielectric constant of the polyethylene plastic that comprises corrugated plastic tubing (CPT) drainage pipe has a value averaging 2.35 (Chemical Rubber Company, 1994).

The GPR unit used predominantly for this research was the Sensors & Software Inc. Noggin<sup>plus</sup> (fig. 3a) (Mississauga, Ontario, Canada) with 250-MHz center frequency antennas. An integrated odometer on the unit measured distance along lines of traverse. In order to investigate the effect of different antenna frequencies on drainage pipe detection, other Sensors & Software Inc. GPR systems were tested in a more limited manner. These included a Noggin<sup>plus</sup>



Figure 3. Ground penetrating radar systems used in this study; (a) Sensors & Software Inc. Noggin<sup>plus</sup> with 250- or 500-MHz center frequency antennas, and (b) Sensors & Software Inc. pulseEKKO 100A with 100- or 200-MHz center frequency antennas.

unit employing 500-MHz center frequency antennas and a pulseEKKO 100A unit (fig. 3b) equipped with 100- or 200-MHz center frequency antennas. The magnitude of the GPR antenna center frequency relates inversely to the depth that the radar pulse penetrates beneath the surface and inversely to the size of the buried object that can be detected. Therefore, choosing the proper antenna frequency based on a buried target's depth and size is extremely important.

A subsurface profile image of the field data was generated for each transect along which GPR measurements were collected. The profile itself is comprised of signal traces typically collected at points a set distance (station interval) of 5 cm (2 in.) apart. Other spatial sampling point distances were tested to a lesser degree for comparison of data quality by setting the station interval at 2.5 or 10 cm (1 or 4 in.). To reduce background noise, 32 signal traces were commonly collected and then averaged (stacked) to produce one signal trace at each point on a line. Background noise tends to be random and can thus be cancelled out by averaging multiple signal traces obtained at the same point. Although data quality can be improved, greater stacking will in turn require a slower survey speed at which GPR measurements can be collected along a transect. Reduced stacking (16, 8, and 4 signal traces averaged at a point location) at sequentially faster survey speeds were studied for assessment of the optimum GPR field operation efficiency at which good quality data could still be obtained.

The horizontal axis on a GPR profile image represents distance along the transect, and the vertical axis gives two-way radar signal travel time in nanoseconds (ns), which can then be converted into depth values. Test plot GPR grid surveys were typically bidirectional in the sense that they were comprised of two sets of parallel transects oriented perpendicular to one another. In almost all cases, the separation distance between transects was 1.5 m (5 ft). For clarity, a generalized schematic of the actual field operational set-up for a GPR grid survey conducted in this study is provided in figure 4. Combined GPR profiles from the grid were then used to produce amplitude maps. These maps correlate with the amount of electromagnetic radar energy reflected back to the surface from a two-way travel time (or depth) interval. Various GPR amplitude maps were generated from subsets of the data collected at several of the test plots (fig. 4) in order to simulate the impact of different field operations, particularly in regard to unidirectional versus

bidirectional surveys and the spacing distance between lines of measurement. Specifically, amplitude maps were produced from data subsets that included bidirectional lines spaced 1.5 m (5 ft) apart, one set of unidirectional lines spaced 1.5 m (5 ft) apart, the second set of unidirectional lines spaced 1.5 m (5 ft) apart, bidirectional lines spaced 3.0 m (10 ft) apart, and bidirectional lines spaced 6.1 m (20 ft) apart.

Computer processing was essential in order to enhance the GPR drainage pipe response embedded in the raw data. The computer processing procedures that were tested included a signal saturation correction filter, gain functions, 2-D migration, signal trace enveloping, a high frequency noise filter, and a spatial background subtraction filter. The signal saturation correction filter removes slowly decaying low frequency noise introduced by factors related to transmitting and receiving antenna proximity and electrical properties of the ground. Gain functions amplify the signal strength, and

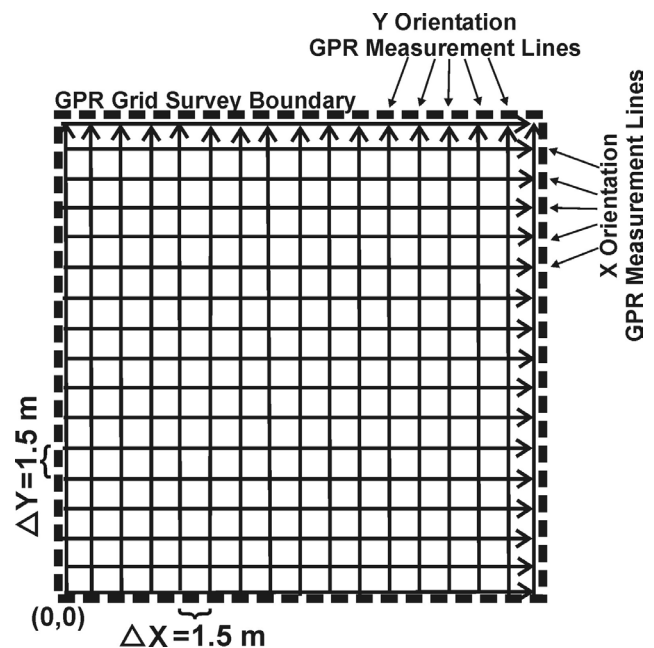


Figure 4. Schematic showing the commonly used field operational set-up for a GPR grid survey conducted in this study. Lines of measurement are bidirectional and spaced 1.5 m apart.

those gain functions that were tried included an automatic gain control, a spreading and exponential compensation gain, a constant gain, and an inverse decay gain. 2-D migration applies a synthetic aperture image reconstruction process that tends to focus scattered signals, and in particular, it collapses hyperbolic GPR responses to point targets. Signal trace enveloping converts the wavelets on the signal trace from ones with both positive and negative components to ones that are monopulse and all positive. As the name implies, the high frequency noise filter reduces the random high frequency components along a signal trace. The spatial background subtraction filter enhances dipping features while suppressing those that are horizontal. All of these computer-processing procedures were extensively tested to determine which combinations were most useful for generating GPR profiles and amplitude maps that reveal the position of buried drainage pipes.

A substantial portion of the research that is being reported was obtained at one test plot. This test plot was built specifically for the project and is located behind the ElectroScience Laboratory (ESL) at Ohio State University (OSU) in Columbus, Ohio. The surface soil (2.5- to 15-cm depth, Ap horizon) at the ESL site, as determined by grain size analysis (Wray, 1986), is classified as silty clay. Figure 5 is a schematic showing the layout of the ESL test plot, which was constructed with both clay tile and CPT drainage pipe placed in 0.5-m (1.5-ft) wide trenches. Due to land slope, depth to the drainage pipe system on its northwest corner was 1 m (3 ft), and 0.6 m (2 ft) on the southeast corner. Shortly following backfill of the trenches where the 10 cm (4 in.) diameter pipes were placed, the test plot was tilled down to a depth of 20 cm (8 in.) so that typical agricultural field conditions could be replicated (fig. 1). Two 10 cm (4 in.) diameter riser pipes (fig. 5) connect the buried drainage pipe system to the surface, thereby allowing a shallow water table to be maintained at any desired level through use of a water supply hose connected to a Hudson valve suspended inside one of the riser pipes.

Due to the ease with which the water table could be raised or lowered, the ESL test plot proved ideal for studying the influence of shallow hydrologic conditions on GPR drainage pipe detection. The shallow hydrologic conditions tested

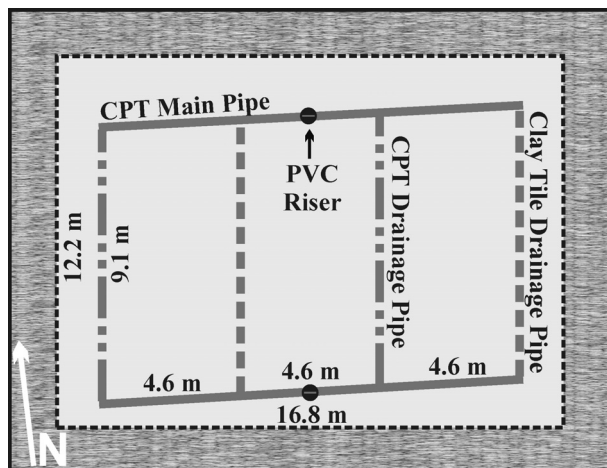


Figure 5. Schematic of the ESL test plot utilized for studying GPR drainage pipe detection. GPR surveys were conducted within the dashed boundary.

included; a) moderately dry soil with a water table beneath the drainage pipes, b) a water table raised 0.5 m (1.5 ft) above the pipes, c) a wet surface and raised water table, d) a very moist soil profile with pipes totally drained of water, and e) frozen ground at the surface below which the soil profile was very moist along with pipes half-full of water. Also, the impacts of antenna frequency, drainage pipe orientation, and drainage pipe material on the GPR response were investigated at the ESL test plot. Furthermore, data from the ESL test plot was used to illustrate the effects of various computer-processing procedures. Additional test plots in central and northwest Ohio were employed to address other considerations regarding equipment parameters such as spatial sampling interval and signal trace stacking, site conditions such as soil texture, drainage pipe orientation, and drainage pipe diameter, and field operations such as unidirectional versus bi-directional GPR surveys and the spacing distance between lines of GPR measurement.

## RESULTS AND DISCUSSION

Research results are presented in figures 6, 7, 8, 9, 10, 11, 12, and 13. Again, the horizontal axis on all ground penetrating radar (GPR) profiles represents distance in meters (m) along the transect where measurements were obtained. The left vertical axis on all profiles gives two-way radar signal travel time in nanoseconds (ns). When conversions could be made and there was space available in the figure, then a right vertical axis was included providing depth values in meters. Both the vertical and the horizontal axes on GPR amplitude maps give distance in meters.

### COMPUTER PROCESSING PROCEDURES

#### *Filters, Gain Functions, Migration, and Signal Trace Enveloping*

Aspects of computer processing are illustrated in figure 6 with GPR profiles and amplitude maps all generated from the same ESL test plot data set. All the GPR data for figure 6 were collected with a station interval of 5 cm (2 in.), a signal trace stacking of 32, and under site conditions in which the surface was frozen, the soil profile below was very moist, and drainage pipes were half-full of water. The GPR profiles shown in figure 6 are labeled with a "1" and were produced from measurements collected along a line perpendicular to the orientation of the four drainage pipes (see fig. 5). If exhibited, GPR drainage pipe responses are highlighted in the figure 6 profiles. The GPR amplitude maps in figure 6 labeled with a "2" correlate to the reflected radar energy for the two-way travel time interval between 20 and 35 ns (depth interval: 0.7 to 1.2 m). Lighter shades on the amplitude maps indicate higher reflected radar energy, and linear features of this nature can suggest the presence of buried drainage pipes. The GPR profile and amplitude map created from the raw data without any additional computer processing are respectively displayed in figures 6a1 and 6a2. Neither the raw data profile (fig. 6a1) nor the amplitude map (fig. 6a2) provides any indication of the presence of buried drainage pipes.

A signal saturation correction filter (SSCF) and a spreading and exponential compensation gain function (SECGF) were applied to the raw data in order to produce the figure 6b1 profile and the figure 6b2 amplitude map. Four different gain functions were tested, but a spreading and

exponential compensation gain, with a start value of 1.0, an attenuation of 7.5 decibels/m, and a maximum gain factor of 500, seemed to be the one that worked best. The figure 6b2 amplitude map gives no indication of the subsurface drainage system present, but the figure 6b1 profile shows four laterally compressed upside-down U-shaped features directly attributable to buried drainage pipes. These features are the typical GPR drainage pipe response shown on gain function processed profiles generated from measurements collected along a transect perpendicular to the trend of a drain line. The apex of one of these upside down U-shaped features, referred

to as “reflection hyperbolas” by geophysicists, denotes the actual position of the top of a buried drainage pipe. It should be noted that other small, isolated buried objects can produce a similar response on a GPR profile (Conyers and Goodman, 1997), and in order to be certain the reflection hyperbola represents a subsurface drainage pipe, comparison of several adjacent parallel profiles or a properly processed test plot amplitude map are needed to see if these features have a linear trend.

Beyond the SSCF and SECGF, creating the figure 6c1 profile and the figure 6c2 amplitude map required the

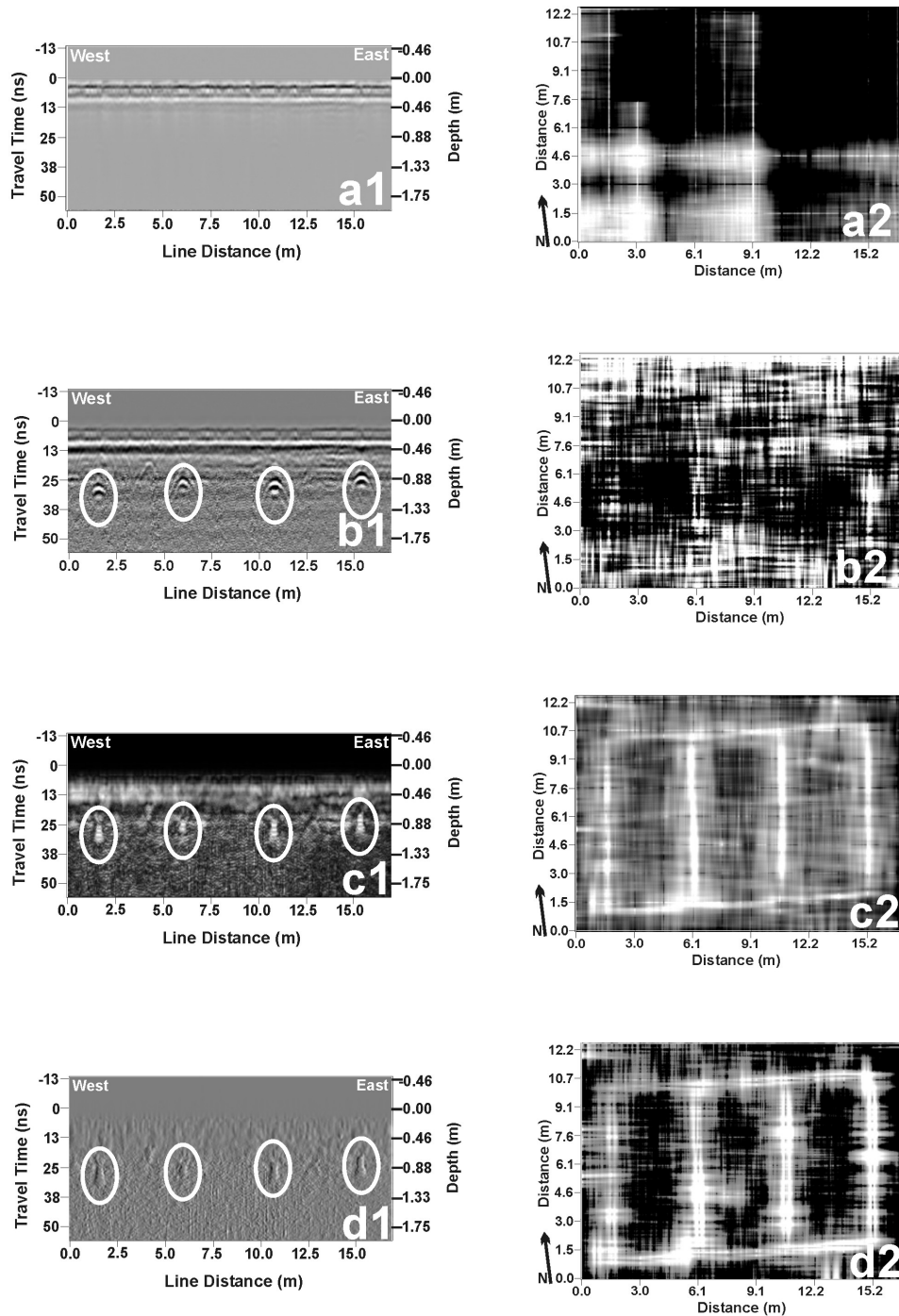


**Figure 6. Computer processing procedures tested for enhancement of the drainage pipe response in ESL test plot GPR profiles and amplitude maps: (a1) and (a2) raw data only; (b1) and (b2) SSCF and SECGF; (c1) and (c2) SSCF, SECGF, 2DM, and STE; and (d1) and (d2) SSCF, SECGF, 2DM, STE, HFNF, and SBSF.**

additional application of 2-D Migration (2DM) based on a field-determined 0.07 m/s soil radar velocity followed by signal trace enveloping (STE). The four drainage pipe reflection hyperbolas shown in the figure 6b1 profile have been essentially collapsed to four points in figure 6c1, but this is not really much of an advantage with regard to determining drainage pipe positions within the GPR profile. 2DM and STE have, however, provided substantial benefits with respect to plotting the subsurface drainage system that is now completely depicted in the figure 6c2 amplitude map.

The figure 6d1 profile and figure 6d2 amplitude map were generated by including a high frequency noise filter (HFNF) and a spatial background subtraction filter (SBSF) along with the prior SSCF, SECGF, 2DM, and STE computer processing steps. The high frequency noise filter applied a three-point running average vertically along each signal trace. The spatial background subtraction filter applied a three-point running average subtraction horizontally across the signal traces. Figure 6d1 shows that adding the HFNF and SBSF obscured the pipe response and therefore should normally not be used to create GPR profiles. At best, the HFNF and SBSF only marginally benefited the figure 6d2 amplitude map depicting the subsurface drainage system.

It is valuable to note that the sequence in which the computer processing steps are employed is very important. The computer processing order for GPR profiles, from beginning to end was: 1<sup>st</sup>, a signal saturation correction filter; 2<sup>nd</sup>, a spreading and exponential compensation gain function; 3<sup>rd</sup>, 2-D migration (if applied); 4<sup>th</sup>, signal trace enveloping (if applied); 5<sup>th</sup>, a high frequency noise filter (if applied); and 6<sup>th</sup>, a spatial background subtraction filter (if applied). The computer processing order for GPR amplitude maps, from beginning to end was: 1<sup>st</sup>, a signal saturation correction filter; 2<sup>nd</sup>, a spreading and exponential compensation gain function; 3<sup>rd</sup>, a high frequency noise filter (if applied); 4<sup>th</sup>, a spatial background subtraction filter (if applied); 5<sup>th</sup>, 2-D migration (if applied); and 6<sup>th</sup>, signal trace enveloping (if applied). Consequently, with respect to the computer processing procedures that best enhance the drainage pipe response in GPR data, a signal saturation correction filter and a spreading and exponential compensation gain function should be used to create profiles, and for amplitude maps, the minimal steps that are needed include a signal saturation correction filter, a spreading and exponential compensation gain function, 2-D migration, and signal trace enveloping. Amplitude maps sometimes warrant further computer processing in the form of a high frequency noise filter and a spatial background subtraction filter. All the GPR profiles and amplitude maps provided throughout the remaining text were generated based on these computer-processing guidelines.

## EQUIPMENT PARAMETERS

### *Antenna Frequency*

Figure 7 shows the GPR response based on different antenna frequencies. The ESL test plot data for figure 7 were collected under dry soil conditions, a station interval of 5 cm (2 in.), and a signal trace stacking of 32. Figures 7a1 and 7a2 were obtained with a pulseEKKO 100A unit and 100-MHz center frequency antennas. Figures 7b1 and 7b2 were obtained with a pulseEKKO 100A unit and 200-MHz center frequency antennas. Figures 7c1 and 7c2 were obtained with

a Noggin<sup>plus</sup> unit and 250-MHz center frequency antennas. Figures 7d1 and 7d2 were obtained with a Noggin<sup>plus</sup> unit and 500-MHz center frequency antennas. For clarity, all GPR drainage pipe responses are highlighted in the figure 7 profiles.

All GPR profiles labeled with a number "1" in figure 7 were produced from measurements obtained along the same line, which was oriented perpendicular to the four north-south trending drainage pipes at the ESL test plot (fig. 5). The reflection hyperbola response to the buried drainage pipes is shown to a greater or lesser extent in figures 7b1, 7c1, and 7d1 with the apex at travel times between 20 and 25 ns. The pulseEKKO 100A unit with 200-MHz center frequency antennas detected all four pipes (fig. 7b1). The Noggin<sup>plus</sup> unit with 250-MHz center frequency antennas detected all four pipes (fig. 7c1), although the response to the one furthest west was subtle. The Noggin<sup>plus</sup> unit with 500-MHz center frequency antennas detected only subtly three of the four pipes (fig. 7d1). The pulseEKKO 100A unit with 100-MHz center frequency antennas detected all four pipes (fig. 7a1), however, the GPR response (at a 20- to 25-ns travel time) to the buried drainage pipes was not the typical reflection hyperbola expected, but rather a rectangular tooth-like extension of the top white band down into the black band beneath it. The difference in GPR drainage pipe response of the pulseEKKO 100A unit with 100-MHz center frequency antennas compared to the other three systems is at present unclear but may be related to reduced object size resolution and interference with radar pulses traveling directly through the air and/or along the ground surface.

All GPR profiles labeled with a number "2" in figure 7 were produced using measurements obtained from the same ESL test plot line, which was oriented directly along trend of one of the buried north-south drainage pipes (the second drain line from the east in fig. 5). The typical GPR response in this scenario is a banded linear feature representing the buried drainage pipe. The position of the top of the banded feature corresponds to the top of the buried drain line. The banded linear feature for the buried north-south drainage pipe shows up quite well around a travel time of 25 ns on the profile generated from data collected using a Noggin<sup>plus</sup> unit with 250-MHz center frequency antennas (fig. 7c2). Figure 7c2 also shows a strong reflection hyperbola on the south end of the banded feature and a subtle one on the north end, both of which represent the corrugated plastic tubing (CPT) main pipe connected at each end of the drainage line (fig. 5). The banded linear feature at a 25-ns travel time is somewhat subtle on the profile generated using a Noggin<sup>plus</sup> unit with 500-MHz center frequency antennas (fig. 7d2). The profile produced using the pulseEKKO 100A unit with 200-MHz center frequency antennas does not show a banded feature representative of the drain line (fig. 7b2). Again, the response of the pulseEKKO 100A unit with 100-MHz center frequency antennas was different. Instead of a distinct linear banded feature, the drain line position is shown by a long rectangular extension of the top white band down into the black band directly beneath it (fig. 7a2).

Choosing the proper antenna frequency based on the subsurface depth and size (diameter) of the drainage pipe is an extremely important consideration. All in all, taking into account different drain line orientations with respect to a GPR transect, the 250-MHz center frequency antennas appeared to work best for detecting buried agricultural

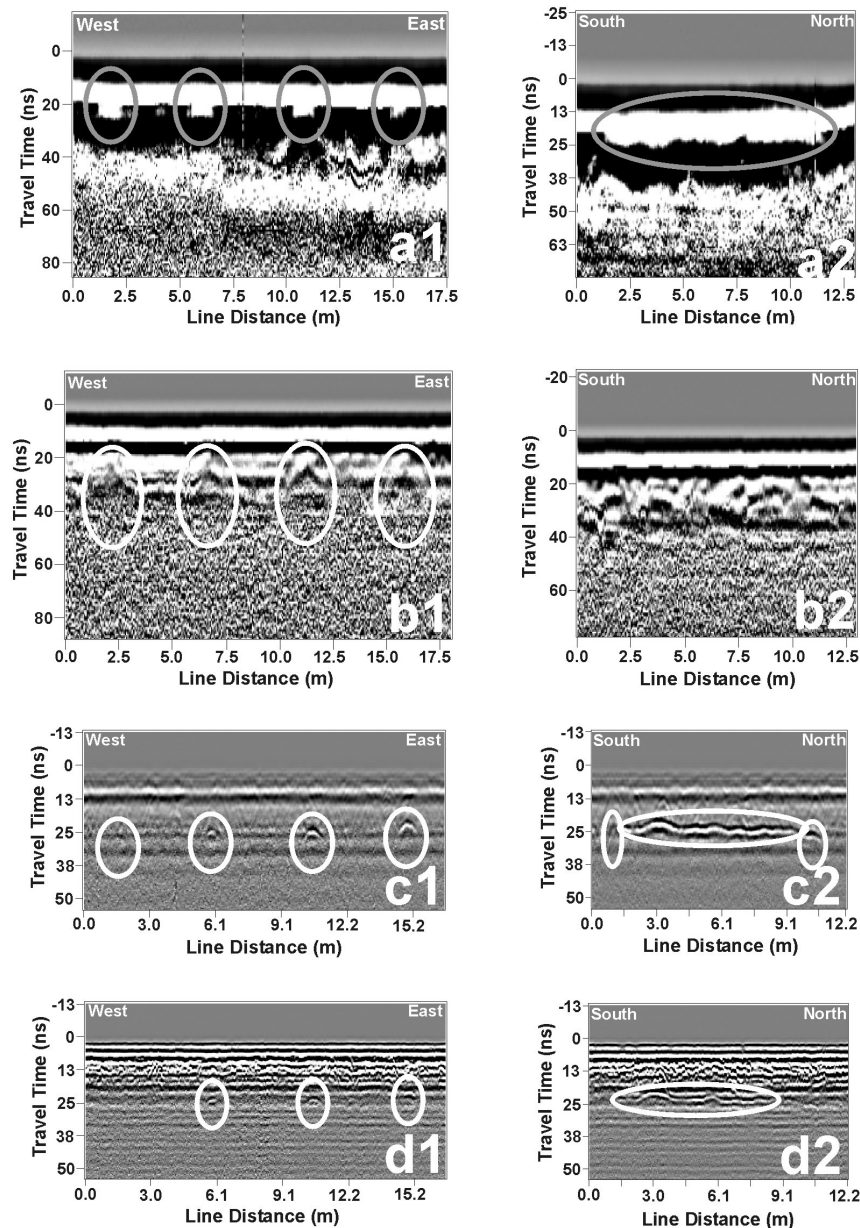


Figure 7. GPR profiles from ESL test plot showing the effect of antenna frequency; (a1) and (a2) pulseEKKO 100A unit with 100-MHz center frequency antennas, (b1) and (b2) pulseEKKO 100A unit with 200-MHz center frequency antennas, (c1) and (c2) Noggin<sup>plus</sup> unit with 250-MHz center frequency antennas, and (d1) and (d2) Noggin<sup>plus</sup> unit with 500-MHz center frequency antennas.

drainage pipe at depths of up to 1 m (3 ft). Perhaps antennas with a 100-MHz center frequency are the best option for larger diameter pipes at greater depth.

#### *Spatial Sampling Interval and Signal Trace Stacking*

Figure 8 depicts the impact on GPR data quality due to spatial sampling interval and signal trace stacking. All four GPR profiles in figure 8 are from a 42.6-m (140-ft) north-south  $\times$  39.6-m (130-ft) east-west test plot located on a portion of the OSU Waterman Agricultural and Natural Resources Laboratory near the intersection of Lane Avenue and Kenny Road in Columbus, Ohio. Soil near the surface (2.5- to 15-cm depth,  $A_p$  horizon), as determined by grain size analysis (Wray, 1986), is at the textural boundary

between clay and silty clay. Two east-west trending subsurface drainage systems are present at this test plot, one comprised of clay tile pipe and the other of corrugated plastic tubing (CPT). The clay tile subsurface drainage system is buried at depths of 0.5 to 1 m (1.5 to 3 ft) and offset 0.6 to 1.8 m (2 to 6 ft) north of the CPT subsurface drainage system, which is 0.6 to 1.2 m (2 to 4 ft) beneath the surface. With its fine-grained soils and the presence of both clay tile and CPT drainage pipes buried at depths ranging from 0.5 to 1.2 m (1.5 to 4 ft), this relatively large test plot proved to be an ideal setting for testing different spatial sampling intervals and signal trace stacking.

GPR measurements for the four profiles (figs. 8a, 8b, 8c, and 8d) were obtained using a Noggin<sup>plus</sup> unit with 250-MHz center frequency antennas along north-south lines oriented

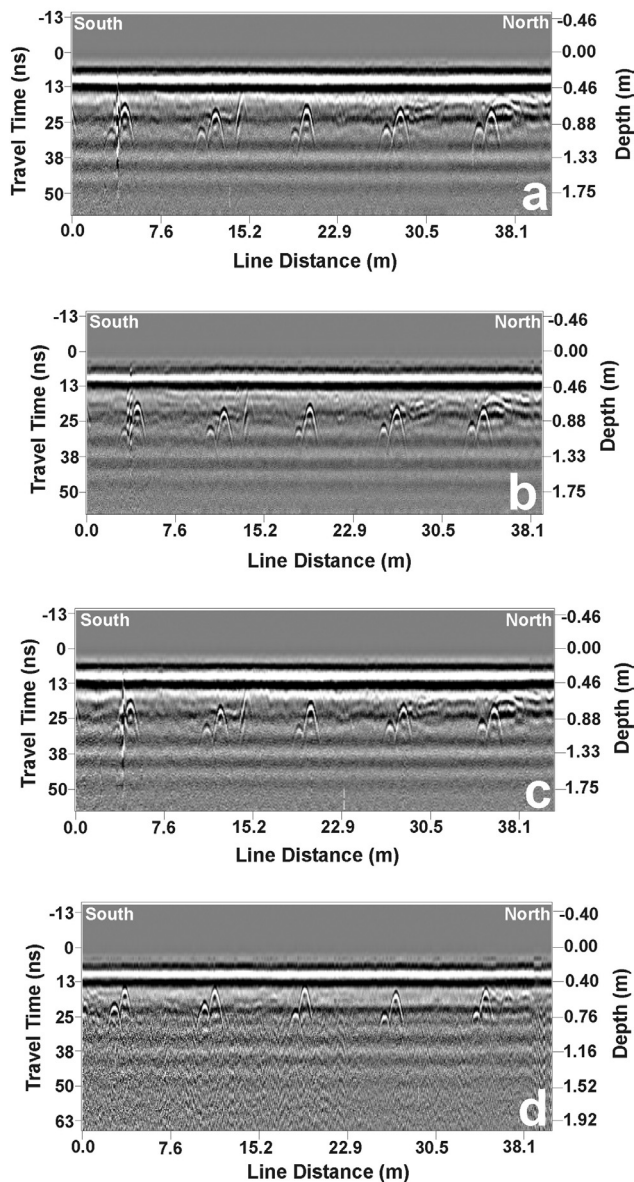


**Figure 8.** GPR profiles showing spatial sampling interval and signal trace stacking effects: (a) station interval equals 2.5 cm and the signal trace stacking is 32, (b) station interval equals 5 cm and the signal trace stacking is 32, (c) station interval equals 10 cm and the signal trace stacking is 32, (d) station interval equals 5 cm and the signal trace stacking is 4.

perpendicular to the general trend of the drainage pipes. The soil profile was moderately wet during data collection. Figures 8a, 8b, and 8c are from the same line near the center of the test plot, and figure 8d is from a line offset 11 m (35 ft) to the west of center.

All four profiles show both the shallow clay tile drainage pipe system and the deeper CPT drainage pipe system. The figure 8a GPR profile was generated from signal traces (stack = 32) collected at points along the line separated 2.5 cm (1 in.) apart. The figure 8b profile was generated from signal traces (stack = 32) collected at points along the line separated 5 cm (2 in.) apart. The figure 8c profile was generated from signal traces (stack = 32) collected at points along the line separated 10 cm (5 in.) apart. The GPR data quality of figures 8a, 8b, and 8c is good and appear relatively similar. This

result may have an important implication, because all other things being equal, reducing the distance (station interval) between points on the line at which signal traces are collected will in turn slow down the speed at which the GPR transect is conducted in order to avoid skipping measurement locations and losing data. Therefore, if good quality GPR data regarding drainage pipe detection can be obtained at a larger spatial sampling interval, then the overall speed of conducting the geophysical survey can be increased.

For most of the research that is being reported, 32 signal traces were averaged (stacked) at each measurement location on a line in order to reduce the random noise that could interfere with the GPR drainage pipe response. For a profile such as figure 8b, in which the station interval was 5 cm (2 in.) and signal trace stacking equaled 32, the slow walking pace at which measurements were collected along the line approached 1.3 km/s (0.8 mph). With this as a starting point, the effect of reduced stacking (16, 8, and 4 signal traces averaged at a point location) at sequentially faster survey speeds was investigated. The figure 8d profile was generated with a station interval of 5 cm (2 in.) and a signal trace stacking of only 4. The measurements for the figure 8d profile line were collected at a speed of around 7.1 km/h (4.4 mph) or at a rate 5.5 times greater than that for the figure 8b profile line, however, the data quality in terms of the GPR drainage pipe detection response is still generally quite good. Consequently, this suggests that, within limits, by reducing the signal trace stacking, GPR survey speeds can be increased to the point, where through integration with a global positioning system (GPS) receiver, large agricultural fields can be efficiently mapped for drainage pipe detection purposes.

## SITE CONDITIONS

### *Shallow Hydrology and Drainage Pipe Material*

The influence of shallow hydrologic conditions on GPR drainage pipe detection is exhibited in figure 9. The data for figure 9 was collected using a Noggin<sup>plus</sup> unit with 250-MHz center frequency antennas. The station interval for this data was 5 cm (2 in.) and the signal trace stacking equaled 32. All GPR profiles in figure 9 labeled with a number “1” were generated from measurements obtained along one line, which was oriented perpendicular to the four north–south trending drainage pipes at the ESL test plot (fig. 5). All GPR profiles labeled with a number “2” in figure 9 were produced from measurements obtained from one ESL test plot line, which was oriented directly along trend of a buried north–south CPT drainage pipe (second drain line from the east in fig. 5). The ESL test plot GPR amplitude maps, which are labeled with a number “3” in figure 9, correlate to the amount of reflected radar energy from a 15 ns time window bracketing the drainage pipe positions.

Figures 9a1, 9a2, and 9a3 correspond to shallow hydrologic conditions with a moderately dry soil profile and a water table below the level of the drainage pipes. The shallow hydrologic conditions for figures 9a1, 9a2, and 9a3 were achieved by covering the ESL test plot with a plastic tarp for over a month prior to the GPR field survey so as to prevent infiltration of rainfall. Figures 9b1, 9b2, and 9b3 correspond to shallow hydrologic conditions with a water table raised 0.5 m (1.5 ft) above the drainage pipes. Figures 9c1, 9c2, and 9c3 correspond to shallow hydrologic conditions with a wet surface from a recent (< 18 h) rainfall of 7.8 mm (0.31 in.) and

a water table raised 0.5 m (1.5 ft) above the drainage pipes. Figures 9d1, 9d2, and 9d3 correspond to shallow hydrologic conditions with a very moist soil profile and pipes totally drained of water. The shallow hydrologic conditions for figures 9d1, 9d2, and 9d3 were obtained by continually pumping water from the drainage pipes and lowering the water table for 24 h prior to the GPR field survey. Figures 9e1,

9e2, and 9e3 correspond to shallow hydrologic conditions with a frozen ground surface, a very moist soil profile below, and drainage pipes half-full of water.

The worst of the shallow hydrologic conditions in regard to GPR drainage pipe detection occur with a static water table located well above the position of the drainage pipes (figs. 9b1, 9b2, and 9b3; figs. 9c1, 9c2, and 9c3). In

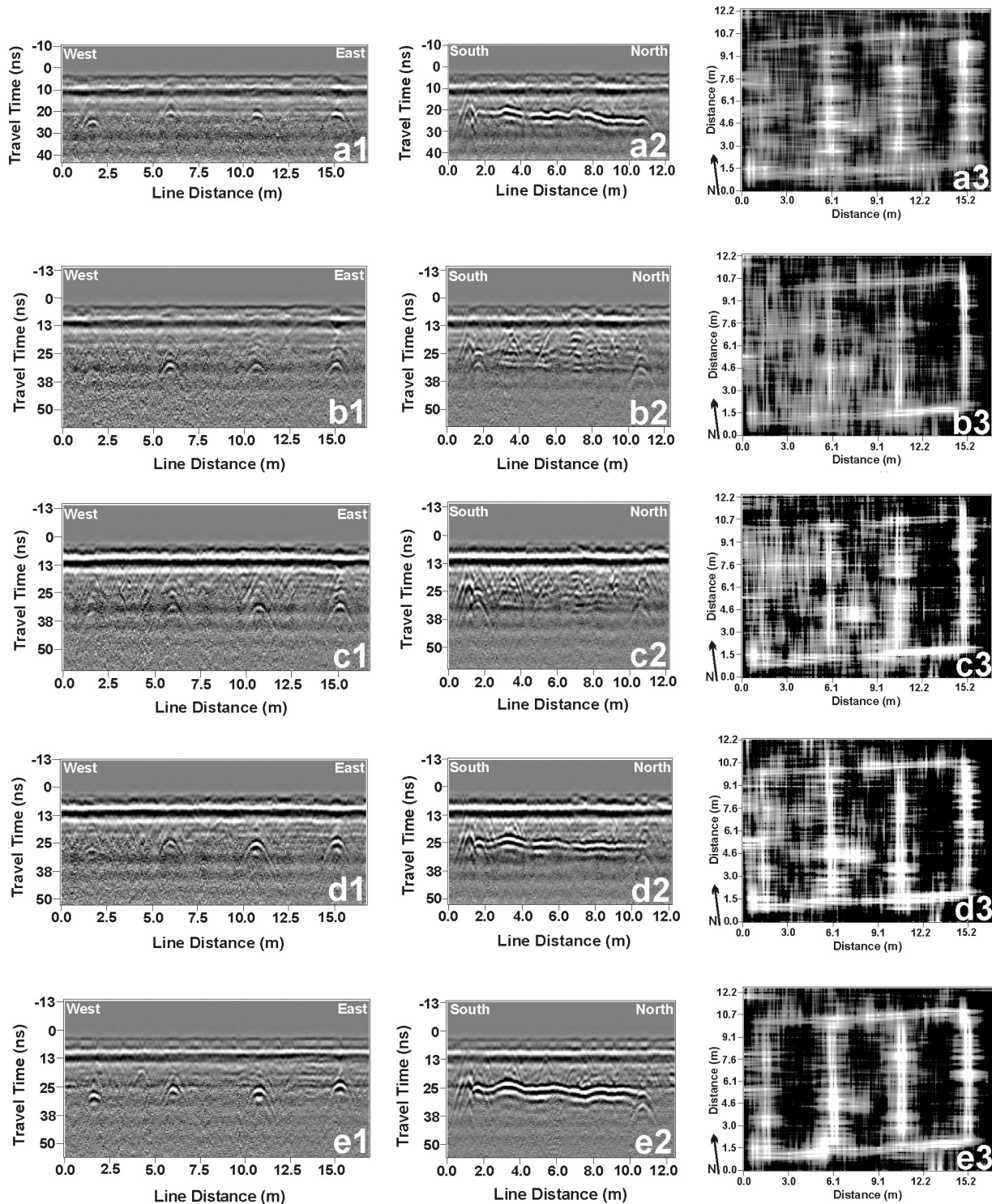


**Figure 9.** ESL test plot GPR profiles and amplitude maps showing the effect of shallow hydrologic conditions: (a1), (a2), and (a3) moderately dry soil with water table below level of drainage pipes, (b1), (b2), and (b3) water table raised 0.5 m above drainage pipes, (c1), (c2), and (c3) wet surface and water table raised 0.5 m above drainage pipes, (d1), (d2), and (d3) a very moist soil profile with drainage pipes totally drained of water, and (e1), (e2) and (e3) frozen ground surface and a very moist soil profile below along with drainage pipes half-full of water.

figures 9b1 and 9c1, the western most of the four drainage pipe reflection hyperbolas is extremely subtle. The banded linear feature representative of a buried drainage pipe oriented directly along trend of the GPR data collection line is almost absent in figures 9b2 and 9c2. Additionally, the subsurface drainage pipe system is difficult to discern on the western end of the GPR amplitude maps provided in figures 9b3 and 9c3. The next best shallow hydrologic condition for GPR drainage pipe detection occurred with a moderately dry soil profile and a water table located below the drainage pipes (figs. 9a1, 9a2, and 9a3), but better yet are conditions with a very moist soil profile surrounding an air-filled drainage pipe (figs. 9d1, 9d2, and 9d3). In figures 9a1 and 9d1, all four of the reflection hyperbolas show up fairly well, but the response is somewhat stronger in figure 9d1. The banded linear feature showing the complete length of a drain line can be seen equally well in figures 9a2 and 9d2. Although subtle in places, the entire subsurface drainage pipe system can be discerned in figure 9a3. The complete subsurface drainage system shows up quite well in figure 9d3. The best of all the shallow hydrologic conditions tested for GPR drainage pipe detection occurred with a frozen ground surface, a very moist soil profile below, and drainage pipes half-full of water (figs. 9e1, 9e2, and 9e3). All four reflection hyperbolas show up very clearly in figure 9e1, and the banded linear feature showing the total length of a drain line is extremely prominent in figure 9e2. Also, the reflection hyperbolas at either end of the banded linear feature are distinct, which are representative of main pipes that connect the drain lines (fig. 5). Likewise, the entire subsurface drainage pipe system is unequivocally defined in figure 9e3.

Soil electrical conductivity is an important factor governing radar signal attenuation, and therefore, its depth of penetration. In essence, radar signal penetration decreases as soil electrical conductivity increases. Soil texture, salinity, and moisture content all influence soil electrical conductivity. As the clay percentage, salinity, and moisture content of a soil increase, so too does its electrical conductivity.

During this portion of the study, in which the effects of shallow hydrologic conditions were being assessed, electromagnetic induction surveys were conducted at the same time the GPR measurements were obtained. A Geophex, Ltd. (Raleigh, N.C.) GEM-2 ground conductivity meter using a primary electromagnetic field frequency of 14610 Hz, at an above ground height of 1 m (3 ft), and in vertical dipole mode, was employed for electromagnetic induction surveying at the ESL test plot. Table 1 provides values of the average ESL test plot soil electrical conductivities for the different shallow hydrologic conditions. As shown in table 1, the average test plot soil electrical conductivities were similar for the shallow hydrologic conditions numbered 1 through 4. These results indicate that changes in soil profile moisture due to rainfall and water table management do not appear to substantially impact soil electrical conductivity. Consequently, dramatic changes in soil electrical conductivity cannot be used to explain the substantially different GPR drainage pipe detection results observed for these four dissimilar shallow hydrologic conditions.

Table 1 indicates that frozen ground surface conditions do affect a significant reduction in the average ESL test plot soil electrical conductivity. This situation occurs because frozen water within the soil has an extremely low electrical conductivity. Since a reduced soil electrical conductivity

**Table 1. Average ESL test plot soil electrical conductivity obtained under different shallow hydrologic conditions.**

Shallow Hydrologic Condition Description	Average ESL Test Plot Soil Electrical Conductivity (mS/m)
1 Moderately dry soil profile and a water table below the level of the drainage pipes	13.77
2 Water table raised 0.5 m above the drainage pipes	15.75
3 Wet surface from a recent rainfall of 7.8 mm and a water table raised 0.5 m above the drainage pipes	16.06
4 Very moist soil profile and pipes totally drained of water	15.50
5 Frozen ground surface, a very moist soil profile below, and drainage pipes half-full of water	7.83

corresponds to less radar signal attenuation, at least for the frozen soil layer near the surface, then this confined zone of decreased electrical conductivity may explain in part the excellent GPR drainage pipe detection results that were obtained under shallow hydrologic conditions in which ground surface was frozen, the soil profile below was very moist, and the drainage pipes were half full of water.

Data collected throughout this study indicates that the type of drainage pipe, whether it is CPT or clay tile, does not significantly influence the GPR drainage pipe detection response. Proof that the GPR drainage pipe detection response does not depend on the type of pipe present can be found in figure 9, by comparing the GPR response of the two north-south drain lines nearest the center of the ESL test plot. Both of these drain lines are placed at about the same depth. The one just west of center is a clay tile drain line, and the one just east of center is a CPT drain line (fig. 5). A separate inspection of the GPR profiles generated from measurements along a transect perpendicular to the trend of the ESL test plot drain lines (figures 9a1, 9b1, 9c1, 9d1, and 9e1) show that, for a given shallow hydrologic condition, the reflection hyperbola response of the center clay tile drain line is almost identical to the reflection hyperbola response of the center CPT drain line.

This similarity also holds up for the drainage pipe response depicted on GPR profiles produced from a line of measurements oriented directly along the trend of a buried drain line. Under conditions of a wet surface and a water table positioned above the drainage pipes, the banded linear feature representing the length of the center CPT drain line is extremely subtle and almost absent in the figure 9c2 profile. Given the same wet surface, raised water table conditions, this observation is also true of the banded linear feature representing the length of the center clay tile drain line shown in figure 10a. With conditions of a frozen ground surface, a very moist soil profile below, and drainage pipes half full of water, the banded linear feature representing the length of the center CPT drain line is very prominent in the figure 9e2 profile. Given the same shallow hydrologic conditions as with figure 9e2, the banded linear feature representing the length of the center clay tile drain line is also very prominent as shown in figure 10b. Finally, regardless of the type of drainage pipe and shallow hydrologic conditions

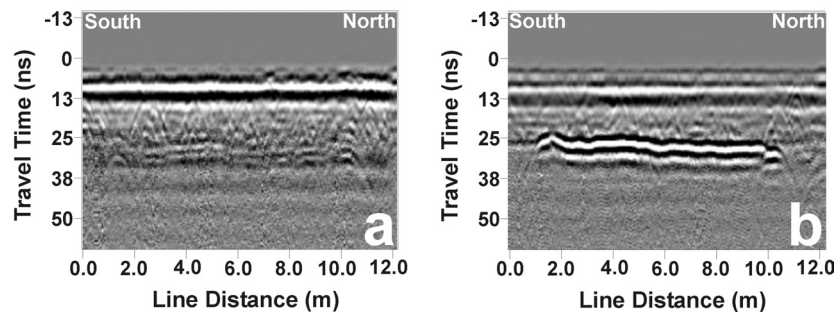


**Figure 10.** ESL test plot GPR profiles along trend of a buried clay tile drain line under different shallow hydrologic conditions: (a) wet surface and water table raised 0.5 m above the drainage pipe, (b) frozen ground surface and a very moist soil profile below along with a drainage pipe half full of water.

present, the GPR drainage pipe response pattern remains consistent. No matter whether the GPR profile response is a reflection hyperbola or a linear banded feature, the color sequence of bands from the top downwards is black–white–black–white–black, with the bottom two bands being the most subtle.

The wall thickness of the pipe compared to the radar pulse wavelength may explain in part why the type of drainage pipe present does not seem to impact the GPR response. The wall thickness of a CPT drainage pipe is approximately 1 mm (0.04 in.), and that of a clay tile drainage pipe is 12.7 mm (0.5 in.). Both of these wall thickness values are quite small compared to the 250–MHz center frequency radar pulse wavelengths that range from 210 to 340 mm (8 to 13 in.) for saturated to moderately dry soils similar to the type found at the ESL test plot (Conyers and Goodman, 1997). Because the pipe wall is thin, a radar pulse travels through it relatively fast. Consequently, just by considering the top half of the drainage pipe, the relatively large wavelength for a 250–MHz radar pulse, and a comparatively small two–way radar signal travel time through the pipe wall, then given these conditions, a phenomena occurs where the radar pulse reflecting off the outer wall and the radar pulse reflecting off the inner wall become superimposed on one another through either constructive or destructive interference. Another possible reason that the GPR drainage pipe response appears not to be affected by the type of pipe present may be due to the similarity in the dielectric constant of the polyethylene in CPT, which is 2.35, and the dielectric constant of dry clay tile, which is around 5. A dielectric constant of 5 for clay tile drainage pipe might be a fairly reasonable assumption (Chemical Rubber Company, 1994; Sharma, 1997), because from personal observation, it has been noticed that drops of water tend to bead up on the surface of a clay tile drainage pipe, indicating that moisture is not readily absorbed.

The previous discussions on soil electrical conductivity and the minimal effect due to the type of drainage pipe present suggest that the GPR drainage pipe detection responses exhibited in figure 9 are most strongly governed by differences in the dielectric constant between the soil surrounding the pipe and the air/water within the pipe. This is particularly true when one considers the disparity in the GPR response for conditions with a saturated soil and water–filled drainage pipe versus those of a very moist soil profile and an air–filled drainage pipe. The absolute value of the reflection coefficient (eq. 1), based only on the soil surrounding the pipe and the air/water contained within the pipe (at least the top half), may be a semi–quantitative way

of gauging the GPR drainage pipe detection response under different shallow hydrologic conditions.

Again, the dielectric constant values for the air or water inside the drainage pipe are respectively, 1 and 80. Equation 3 can be used to calculate the dielectric constant under different moisture conditions for glacially derived soils common throughout the Midwest United States. This equation was therefore employed to approximate dielectric constant values for the silty clay soil present at the ESL test plot. Given moderately dry conditions with a volumetric moisture content estimated to be 0.2, the calculated dielectric constant for this soil is around 15. The dielectric constant is 30 for very moist conditions (near field capacity) where the estimated volumetric moisture content is 0.4. The dielectric constant is around 40 for saturated conditions, assuming a total soil porosity of 0.5. Even after a day or two of drainage, with the overall soil profile near field capacity and the water table at or just below the drainage pipes, capillary processes will still keep the silty clay ESL soil immediately surrounding the pipe in a saturated condition. Consequently, only in those cases that were applicable, the reflection coefficient was calculated using a saturated soil dielectric constant value instead of one for a very moist soil near field capacity.

The absolute value of the reflection coefficient based only on the surrounding soil and the air or water inside the pipe is 0.59 for a moderately dry soil with an air–filled pipe, 0.73 for a saturated soil with an air–filled pipe, and 0.17 for a saturated soil with a water–filled pipe. These reflection coefficient calculations compared with one another seem to correspond well with respect to the strength of the GPR drainage pipe response shown in figure 9 for different shallow hydrologic conditions. Therefore, the absolute value of the reflection coefficient, based on the soil immediately surrounding the pipe and the air/water within it, can provide insight and help gauge the potential impact of shallow hydrologic conditions on GPR drainage pipe detection.

The results for this portion of the study provide some important guidelines as to when a GPR drainage pipe mapping survey should be conducted with regard to the shallow hydrologic conditions present. Clearly, GPR surveys should be avoided when the water table is above the elevation of the drainage pipes. This shallow hydrologic condition takes place most often in the hours (or day or two at most) directly following a substantial rainfall event and before much soil drainage has occurred. Although less typical, the water table is also elevated above the drainage pipes, usually for prolonged periods of time, at locations where controlled drainage and/or subirrigation methods are in use. Moderately dry soils with the water table at or below the drain lines (pipes

are completely or at least largely air-filled) are an acceptable shallow hydrologic condition for the use of GPR to locate drainage pipes. The moderately dry soil, low water table condition is fairly common during periods where there has been little rainfall. A better shallow hydrologic condition for GPR drainage pipe detection occurs with a very moist soil profile and a water table at or below the drain lines (pipes are completely or at least largely air-filled). The very moist soil, low water table conditions often occur during wet periods, especially a day or two following a significant rainfall event, after which most of the excess soil water has had a chance to drain. Better yet in terms of GPR drainage pipe detection are shallow hydrologic conditions characterized by a frozen ground surface, a very moist soil profile, and a water table at or below the drain lines (pipes are completely or at least largely air-filled). Within the Midwest United States, there are frequent occasions during the winter months that the ground surface is frozen, the soil below is very moist, and the water table is low. Winter also is an ideal time for GPR drainage pipe detection in some other respects, because the crop cover has been removed, agricultural operations have ceased until early spring, and the frozen ground surface greatly improves field accessibility, assuming there is not a substantial amount of snow present. These shallow hydrologic condition GPR guidelines are most applicable to situations common to Ohio, where the soils are typically fine-grained and the drainage pipe placement depths are generally within 1 m (3 ft) of the surface.

#### Soil Type and Drainage Pipe Orientation

Figure 11 compares GPR drainage pipe detection capabilities with respect to the soil texture that is present. In addition, figure 11 further details the GPR response in relation to the orientations of the drainage pipe and the line along which GPR measurements were taken. The data for figure 11 was collected with a Noggin<sup>plus</sup> unit and 250-MHz center frequency antennas at four different test plots in central and northwest Ohio. The station interval was set at 5 cm (2 in.) and the signal trace stacking equaled 32.

The soil texture for figure 11a is a silty clay and the four drainage pipes, as indicated by the laterally tight reflection hyperbolas, were oriented perpendicular to the line along which data was collected. The soil textures at the test plot for figure 11b range from clay to silty clay and the laterally very broad, downward tapering GPR pipe response at around a 20-ns travel time is due to the small angular difference of 4° between the orientations of the measurement transect and the horizontal trend of the drain line. The soil texture for figure 11c is a sandy loam. As shown in figure 11c, strong radar reflections off of layers within the soil profile tend to obscure the four highlighted laterally tight reflection hyperbola responses to drainage pipes that trend perpendicular to the GPR transect. The soil texture for figure 11d ranges from sandy clay loam to sandy loam. Figure 11d is rather complex showing two linear banded features, one at the east end (~25-ns travel time) of the profile and a second at the west end (25- to 38-ns travel time) of the profile. In addition, within the center of the figure 11d profile, there is a highlighted somewhat laterally extended reflection hyperbola. This profile configuration was due to the GPR transect directly following along one drainage pipe on the east end of the line and along another on the west end of the line, while

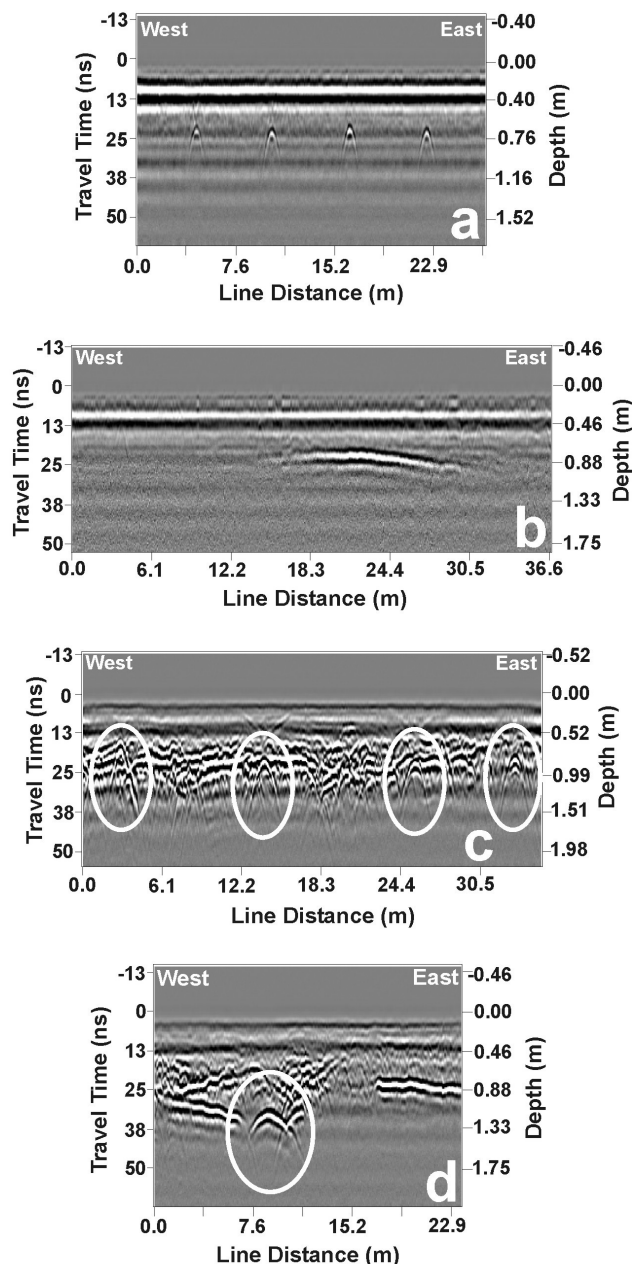


Figure 11. These GPR profiles from central and northwest Ohio test plots show soil texture and pipe orientation effects: (a) silty clay, (b) clay to silty clay, (c) sandy loam, and (d) sandy clay loam to sandy loam.

in the middle of the line, crossing over a third drainage pipe at a horizontal angle of 35°. There are also strong radar reflections off of soil profile layers in figure 11d, but these reflective layers are at a higher level than where the pipes are present, so there is very little interference between them.

Sandy soils tend to have a lower electrical conductivity, and therefore, because of less signal attenuation, are often good environments for GPR investigations. However, figure 11c shows that sandy soils can still become problematic for GPR drainage pipe detection when soil layers that strongly reflect radar energy are at the same level as the drainage pipes. This particular difficulty does not seem to be encountered with soils that are overall more fine-grained (figs. 11a and 11b). The highly reflective layers in a sandy soil

may be due to thin beds of silty/clayey material having a higher water holding capacity than the surrounding coarse-grained sediments, thereby producing dielectric constant discontinuities in the subsurface. Sometimes, a spatial background subtraction filter can be employed during computer processing of the data to remove horizontal layer features within the GPR profile, thereby emphasizing reflection hyperbola responses that are representative of drainage pipes. The downside of this approach is that it can filter out linear-banded features representative of a drainage pipe having the same trend as the line along which GPR measurements were collected.

Figure 11 also emphasizes that the GPR drainage pipe response ranges from a linear banded feature, when the measurement transect follows directly along trend over a drain line, to a laterally tight reflection hyperbola, when the measurement transect crosses over a drainage pipe at a right angle. When the horizontal angle between the GPR measurement transect and the drainage pipe orientation is greater than  $0^\circ$  and less than  $90^\circ$ , the reflection hyperbola becomes spread out laterally to a greater or lesser extent. Consequently, even within a single profile, there are clues as to drainage pipe orientation based on the GPR response.

### Drainage Pipe Diameter

Although somewhat atypical, agricultural drainage pipes that have a diameter smaller than 10 cm (5 in.) are occasionally encountered. One of the test locations in northwest Ohio afforded the opportunity to assess whether the Noggin<sup>plus</sup> unit with 250-MHz center frequency antennas could detect these smaller agricultural drainage pipes in a silty clay soil. This location had two fields that were side by side, one with 10-cm (4-in.) diameter drainage pipes spaced 6 m (20 ft) apart, and the second with 5-cm (2-in.) diameter drainage pipes also spaced 6 m (20 ft) apart. Depths for the 10- and 5-cm (4- and 2-in.) diameter pipes were similar. The station interval was set at 5 cm (2 in.) and signal trace stacking equaled 32 for all site data collected.

Figure 12 shows GPR profiles from two different measurement transects oriented perpendicular to the trend of the drainage pipes. The southern measurement transect extended southeast to northwest from the center to the edge of the field with the 10-cm (4-in.) diameter drainage pipes (fig. 12a1) and then from the edge to the center of the field with the 5-cm (2-in.) diameter drainage pipes (fig. 12a2). In a similar manner, the northern measurement transect extended southeast to northwest from the center to the edge of the field with the 10-cm (4-in.) diameter drainage pipes (fig. 12b1) and then from the edge to the center of the field with the 5-cm (2-in.) diameter drainage pipes (fig. 12b2).

By comparing figure 12a1 with figure 12a2 and then figure 12b1 with figure 12b2, it appears that the Noggin<sup>plus</sup> unit with 250-MHz center frequency antennas detected both the 10-cm (4-in.) diameter drainage pipes and the 5-cm (2-in.) diameter drainage pipes equally well. On the southern transect, where the GPR profile drainage pipe response was strong for the 10-cm (4-in.) diameter pipes (fig. 12a1), it was also strong for the 5-cm (2-in.) diameter pipes (fig. 12a2). Likewise, on the northern transect, where the GPR profile drainage pipe response was subtle for the 10-cm (4-in.) diameter pipes (fig. 12b1), it was also subtle for the 5-cm (2-in.) diameter pipes (fig. 12b2). Consequently, at least for

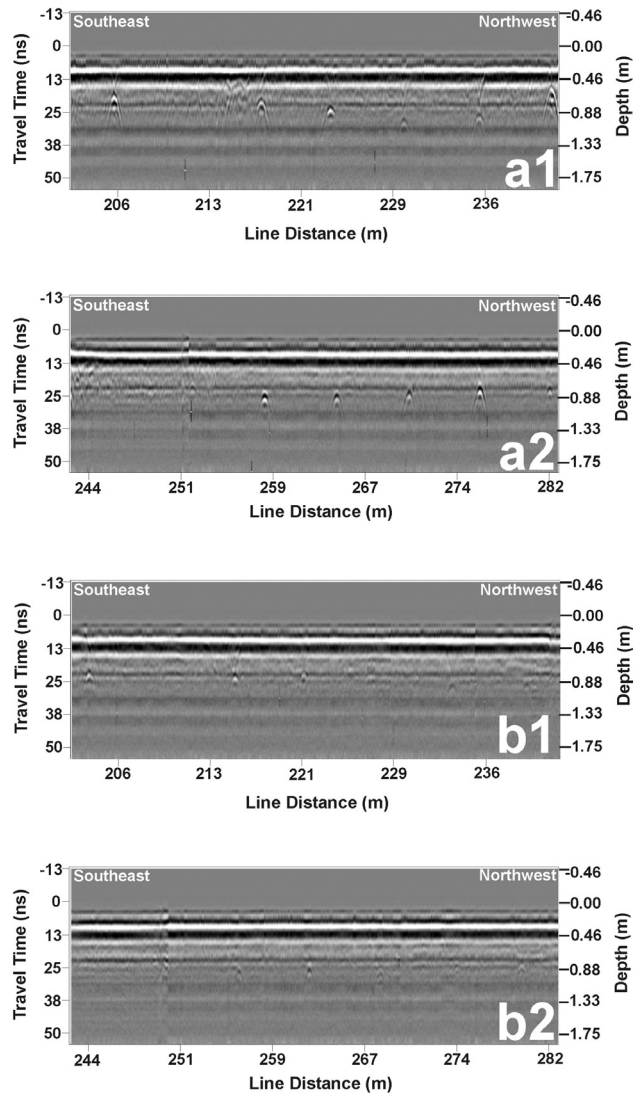


Figure 12. GPR profiles comparing the response of different diameter drainage pipes: (a1) south transect, 10-cm diameter pipes, (a2) south transect, 5-cm diameter pipes, (b1) north transect, 10-cm diameter pipes, and (b2) north transect, 5-cm diameter pipes.

depths of 1 m (3 ft) or less, the Noggin<sup>plus</sup> unit with 250-MHz center frequency antennas appears fairly capable of detecting buried drainage pipes with diameters as small as 5 cm (2 in.).

### FIELD OPERATIONS

#### Unidirectional Versus Bidirectional Surveys and GPR Measurement Line Spacing Distance

Issues related to field operations need to be considered before setting up a GPR grid survey to map subsurface drainage systems. Particularly important are decisions regarding whether a unidirectional or bidirectional survey is to be conducted and the spacing distance to use between lines along which GPR measurements are obtained. Figure 13 demonstrates the impact of these GPR field operation decisions. The data for figure 13 was collected at a test plot in northwest Ohio with a Noggin<sup>plus</sup> unit and 250-MHz center frequency antennas. The station interval was set at 5 cm (2 in.) and signal trace stacking equaled 32. Soil at the surface (2.5- to 15-cm depth, Ap horizon) of this test plot is

classified as sandy clay loam to sandy loam based on grain size analysis (Wray, 1986). For almost every case in this investigation, test plot GPR grid surveys were bidirectional with a spacing distance of 1.5 m (5 ft) between measurement transects (fig. 4). Subsets of a test plot data set, of which figure 13 is only one example, can be utilized to simulate the impact of different field operations on GPR drainage pipe mapping, particularly in regard to unidirectional versus

bidirectional surveys and the spacing distance between lines of measurement.

Figure 13a is a schematic showing the drainage pipe layout at the test plot. All figure 13 GPR amplitude maps of the test plot subsurface drainage system were produced using a two-way travel time interval of 23 to 40 ns (depth interval: 0.8 to 1.4 m). Figure 13b is an amplitude map based on an east–west and north–south bidirectional survey with lines of

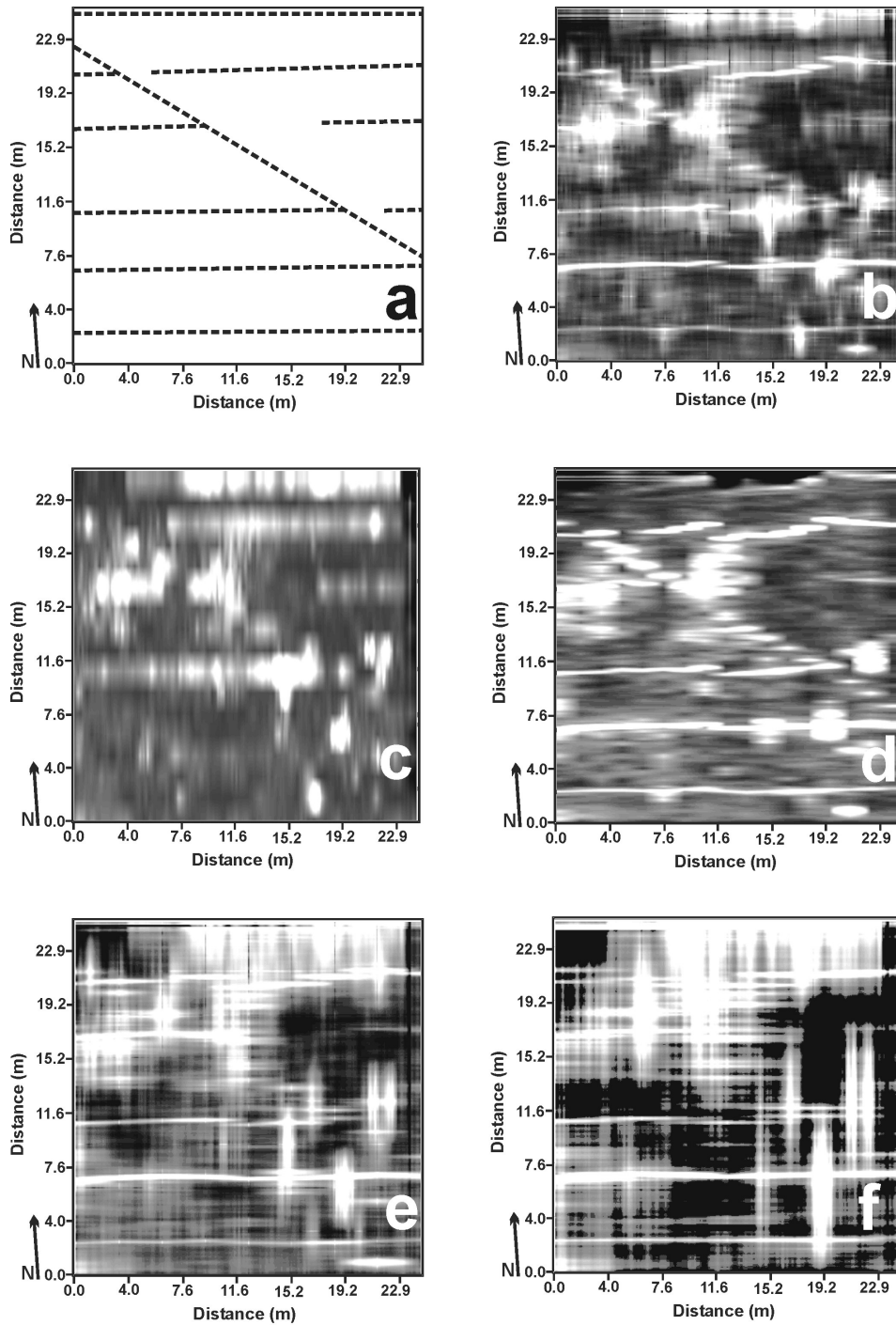


**Figure 13.** GPR survey field operation impacts on an amplitude map depicting an agricultural subsurface drainage system: (a) schematic of the subsurface drainage system pattern in dashed lines, (b) map based on bidirectional survey with measurement lines spaced 1.5 m apart, (c) map based on east–west unidirectional survey with measurement lines spaced 1.5 m apart, (d) map based on north–south unidirectional survey with measurement lines spaced 1.5 m apart, (e) map based on bidirectional survey with lines spaced 3.0 m apart, and (f) map based on bidirectional survey with lines spaced 6.1 m apart.

GPR measurement spaced 1.5 m (5 ft) apart. Figure 13c is an amplitude map based on an east–west unidirectional survey with measurement lines spaced 1.5 m (5 ft) apart. Figure 13d is an amplitude map based on a north–south unidirectional survey with measurement lines spaced 1.5 m (5 ft) apart. Figure 13e is an amplitude map based on an east–west and north–south bidirectional survey with measurement lines spaced 3.0 m (10 ft) apart. Figure 13f is an amplitude map based on an east–west and north–south bidirectional survey with measurement lines spaced 6.1 m (20 ft) apart.

Perhaps most significant from figure 13 is the demonstrated need to conduct bidirectional surveys with one set of parallel GPR measurement lines perpendicular to a second set of parallel GPR measurement lines. Conducting only a unidirectional survey runs the risk of completely missing some of the drainage pipes present, especially if the one set of GPR measurement transects is fairly close to being parallel with the trend of the drain lines (fig. 13c). Figures 13b, 13e, and 13f show that the subsurface drainage system becomes more poorly defined on an amplitude map as the spacing between lines of GPR measurement is increased from 1.5 to 3.0 to 6.1 m (5 to 10 to 20 ft). Although, even the amplitude map generated with a spacing distance of 6.1 m (20 ft) between transects (fig. 13f) still contains plenty of useful information on the subsurface drainage system present. It should be noted that generating an amplitude map is extremely helpful, but not necessarily required in order to ascertain the layout of the subsurface drainage system. There are times when a few GPR profiles from measurement transects, of which some are perpendicular to one another, are all that is needed.

## SUMMARY

Locating buried agricultural drainage pipe is an important problem confronting farmers and land improvement contractors in the Midwest United States. Ground penetrating radar (GPR) may provide a solution. Results from initial research found GPR to be successful in locating on average 72% of the total amount of pipe present at 13 test plots in southwest, central, and northwest Ohio. The effective use of GPR for drainage pipe detection requires careful consideration of computer processing procedures, equipment parameters, site conditions, and field operations, all of which were addressed in some detail during this continuing investigation. Some of the more important results obtained include the following.

- 1 Application of a signal saturation correction filter along with a spreading and exponential compensation gain function were the computer processing steps found to be most helpful for enhancement of the drainage pipe response exhibited within GPR images of the soil profile.
- 2 GPR amplitude maps that show the overall subsurface drainage pipe system required additional computer processing, which included 2–D migration, signal trace enveloping, and in some cases, a high frequency noise filter and a spatial background subtraction filter.
- 3 A GPR unit with 250–MHz center frequency antennas seemed to work best for detecting buried agricultural drainage pipe under conditions typical in Ohio.
- 4 Within limits, increasing the spatial sampling interval and reducing signal trace stacking still produces good quality data, while at the same time increasing the speed at which a GPR survey can be conducted.
- 5 Shallow hydrologic conditions with a saturated soil surrounding a water–filled drainage pipe produce the poorest GPR drainage pipe detection response.
- 6 Shallow hydrologic conditions with a wet/saturated soil surrounding an air–filled drainage pipe produce the best GPR drainage pipe detection response, especially if the ground surface is frozen.
- 7 The type of drainage pipe present, either clay tile or corrugated plastic tubing, does not seem to impact the GPR response.
- 8 The orientation of the drain line, from parallel to perpendicular, with respect to the transect along which measurements are collected, is what governs the GPR profile pipe response that ranges, respectively, from a banded linear feature to a laterally extended reflection hyperbola to a laterally compressed reflection hyperbola.
- 9 Sandy soils often have layers that strongly reflect radar energy, which in turn can potentially interfere with drainage pipe detection.
- 10 GPR is capable of detecting drainage pipes having a diameter as small as 5 cm (2 in.).
- 11 To avoid missing some of the drainage pipes that are present at an agricultural field site, bidirectional GPR surveys should be conducted that are comprised of two perpendicular sets of parallel measurement lines.
- 12 The layout of a subsurface drainage system on an amplitude map becomes more poorly defined as the spacing distance between GPR measurement lines is increased.

As an end product, this research study has accumulated a wealth of information that can be used directly as guidelines to improve the potential for success of using ground penetrating radar to locate buried agricultural drainage pipe.

## ACKNOWLEDGEMENTS

Most of the funding for this research project was provided through a grant from the Ohio State University – Ohio Agricultural Research and Development Center. Substantial additional support came from the U.S. Department of Agriculture – Agricultural Research Service.

## REFERENCES

- Allred, B. J., N. R. Fausey, L. Peters, Jr., C. Chen, J. J. Daniels, H. Youn. 2004. Detection of buried agricultural drainage pipe with geophysical methods. *Applied Engineering in Agriculture* 20(3): 307–318.
- Boniak, R., S. K. Chong, S. J. Indorante, and J. A. Doolittle. 2002. Mapping golf course green drainage systems and subsurface features using ground penetrating radar. In *Proc. of SPIE, Ninth International Conference on Ground Penetrating Radar*, vol. 4758, eds. S. K. Koppenjan and H. Lee, 477–481. Santa Barbara, Calif.: SPIE.
- Chemical Rubber Company. 1994. *CRC Handbook of Chemistry and Physics*, ed. D. R. Lide. Boca Raton, Fla.: CRC Press.

- Chen, H., H. H. Xu, and Y. Hu. 1991. Detecting underground cables and metal conducting pipes using EM methods. In *Investigations in Geophysics No. 5, Geotechnical and Environmental Geophysics, V. 3, Geotechnical*, ed. S. Ward, 229–237. Tulsa, Okla.: Soc. Exploration Geophysicists.
- Chow, T. L., and H. W. Rees. 1989. Identification of subsurface drain locations with ground-penetrating radar. *Can. J. Soil Sci.* 69: 223–234.
- Conyers, L. B., and D. Goodman. 1997. *Ground-Penetrating Radar: An Introduction for Archaeologists*. Walnut Creek: AltaMira Press.
- Hayakawa, H., and A. Kawanaka. 1998. Radar imaging of underground pipes by automated estimation of velocity distribution versus depth. *J. Applied Geophysics* 40: 37–48.
- LaFaleche, P. T., J. P. Todoeschuck, O. G. Jensen, and A. S. Judge. 1991. Analysis of ground probing radar data: Predictive deconvolution. *Canadian Geotechnical J.* 28(1): 134–139.
- Peters, Jr., L., and J.D. Young. 1986. Applications of subsurface transient radar. In *Time Domain Measurements in Electromagnetics*, ed. E. K. Miller, 297–351. New York: Van Nostrand Reinhold.
- Reynolds, J. M. 1997. *An Introduction to Applied and Environmental Geophysics*. Chichester, United Kingdom: John Wiley & Sons.
- Schwab, G. O., R. K. Frevert, T. W. Edminster, and K. K. Barnes. 1981. *Soil and Water Conservation Engineering*, Third Edition. New York: John Wiley & Sons.
- Sharma, P. V. 1997. *Environmental and Engineering Geophysics*. Cambridge, United Kingdom: Cambridge University Press.
- Sutinen, R. 1992. Glacial deposits, their electrical properties and surveying by image interpretation and ground penetrating radar. Bulletin 359. Geological Survey of Finland. Rovaniemi, Finland.
- Topp, G. C., J. L. Davis, and A. P. Annan. 1980. Electromagnetic determination of soil water content: Measurements in coaxial transmission lines. *Water Resources Research* 16(3): 574–582.
- USDA. 1987. Economic Research Service. Farm Drainage in the United States: History, Status, and Prospects. USDA Miscellaneous Publication 1455. Washington, D.C.: USDA.
- Wensink, W. A., J. Hofman, and J. K. Van Deen. 1991. Measured reflection strengths of underwater pipes irradiated by pulsed horizontal dipole in air: Comparison with continuous plane-wave scattering theory. *Geophysical Prospecting* 39(4): 543–566.
- Wray, W. K. 1986. *Measuring Engineering Properties of Soil*. Englewood Cliffs, N.J.: Prentice-Hall, Inc.
- Young, J. D., and R. Caldecott. 1976. Underground pipe detector. U.S. Patent 3,967,282.
- Zeng, X., and G. A. McMechan. 1997. GPR characterization of buried tanks and pipes. *Geophysics* 62(3): 797–806.
- Zhang, G., and Y. Luo. 1991. The application of IP and resistivity methods to detect underground metal pipes and cables. In *Investigations in Geophysics No. 5, Geotechnical and Environmental Geophysics, V. 3, Geotechnical*, ed. S. Ward, 239–248. Tulsa, Okla.: Soc. Exploration Geophysicists.
- Zucker, L. A., and L. C. Brown, Editors. 1998. Agricultural drainage: Water quality impacts and subsurface drainage studies in the Midwest. Ohio State University Extension Bulletin 871. Columbus, Ohio: The Ohio State University.

## NOMENCLATURE

GPR	=	ground penetrating radar
CPT	=	corrugated plastic tubing
R	=	radar signal reflection coefficient (dimensionless)
$\epsilon$	=	dielectric constant (dimensionless)
$\theta$	=	volumetric moisture content (dimensionless)
SSCF	=	signal saturation correction filter
SECGF	=	spreading and exponential compensation gain function
2DM	=	2-D migration
STE	=	signal trace enveloping
HFNF	=	high frequency noise filter
SBSF	=	spatial background subtraction filter

